Atmospheric Correction for NO_2 Absorption in Retrieving Water-Leaving Radiances from the SeaWiFS and MODIS Measurements

Z. Ahmad[1,2], C. R. McClain[1], J. R. Herman[1], B. Franz[1,3], E. Kwiatkowska[1,3], W. Robinson[1,3], E. J. Bucsela[1,4], and M. Tzortziou[1,5]

[1]NASA Goddard Space Flight Center, Greenbelt, Maryland, USA
[2]Science and Data Systems, Inc., Silver Spring, Maryland, USA
[3]Science Applications International Corporation, San Diego, California, USA
[4]University of Maryland, Baltimore County, Maryland, USA
[5]University of Maryland, College Park, Maryland, USA

INTRODUCTION

NO_2 is an important trace gas that plays a major role in the destruction of ozone in the middle stratosphere, and production of ozone in the lower troposphere (Solomon *et al*., 1999). In the stratosphere, the NO_2 is mainly produced by photo-dissociation of the NO_2 reservoir species. In the lower troposphere (1 to 3 km), the primary sources of NO_2 production are, industries (power generation ~25%), automobiles (~50%) and biomass burning. These sources together with emission from the soil, account for most of the NO_2 in the atmosphere.

NO_2 has a broad absorption spectrum that extends from UV (~270 nm) to the near IR (~770 nm) with a peak in the blue region (Vandaele *et al*., 1998). Until recently, the importance of NO_2 absorption has been largely ignored in the retrieval of oceanic parameters from satellite measurements. For example, in the retrieval of water-leaving radiances from Sea-viewing Wide Field-of-view Sensor (SeaWiFS) and Moderate-Resolution Imaging Spectroradiometer (MODIS) measurements, the effect of NO_2 absorption is not considered at all. Results from Global Ozone Measuring Experiment (GOME), Scanning Imaging Absorption Spectrometer for Atmospheric Cartography (SCIAMACHY) and, most recently, from the Ozone Measuring Instrument (OMI) sensors clearly show the presence of NO_2 near the Eastern Coast of the US and Northern Europe. Over the Eastern US the NO_2 column amount often exceeds ~$2x10^{16}$ molecules/cm^2, and shows a seasonal cycle with a maximum in the winter months. In addition, boundary layer NO_2 has a strong diurnal variation with a maximum at around 10 AM in the morning and a gradual decrease throughout the afternoon. There can be significant daily variation in this pattern depending on the daily meteorology and on the strength of the sources (Cede et al., 2006).

Our radiative transfer sensitivity calculations show that, under high NO_2 conditions, the error in the top-of-the-atmosphere (TOA) radiances in the blue channels of the SeaWiFS and MODIS instruments is around one percent. This translates into approximately 10 percent error in water leaving radiance for clear waters. As these water-leaving radiances decrease with an increase in chlorophyll, CDOM amount, and non-algal suspended particles near the coast, the relative error in the water-leaving radiances increases.

In this paper, we report the results of a sensitivity study that examines how the TOA reflectances change with the changes in the NO_2 amount in the troposphere, and provide details of an NO_2 correction algorithm that enables accurate retrieval of water-leaving radiances in the presence of varying amount of NO_2 concentration over the ocean. Also, we have applied the NO_2 atmospheric correction algorithm to many MODIS scenes off the Eastern Coast of the US with large amount of

NO_2 in the atmosphere and found significant increase (~20 percent) in the values of the water-leaving radiances.

RADIATIVE TRANSFER SIMULATIONS (FORWARD MODELING)

Following the radiative transfer (RT) theory, it is customary to write the top-of-the atmosphere (TOA) reflectance, ρ_t, over a rough ocean surface as:

$$\rho_t(\lambda, \theta_o, \theta, \varphi, v) = \rho_{path}(\lambda, \theta_o, \theta, \varphi) + t_1\rho_g(\lambda, \theta_o, \theta, \varphi, v) + t_2\rho_w(\lambda, \theta_o, \theta, \varphi, v) + t_3\rho_{wc}(\lambda,\theta_o, \theta, \varphi, v) \quad (1)$$

Where, λ, θ_o, θ, φ, and v, respectively, refer to the wavelength, the solar zenith angle, the sensor view and azimuth angles, and the wind speed over the ocean surface. ρ_{path}, is the path reflectance to the sensor due to multiple scattering in the atmosphere by air molecules (Rayleigh scattering) and aerosols (Mie scattering). ρ_{path} also includes the contribution from photons that go through both the Rayleigh and the Mie scattering. Also, in Equation 1, ρ_g, ρ_w, and ρ_{wc}, respectively, are, the glint (ρ_g), the water leaving (ρ_w) and white cap (ρ_{wc}) reflectances at the ocean surface, and t_1, t_2, t_3 are their respective transmittances in the direction (θ, φ) through the atmosphere. Here, reflectance is defined as:

$$\rho(\lambda, \theta_o, \theta, \varphi, v)=\pi L(\lambda,\theta_o, \theta, \varphi, v)/\mu_o F_o(\lambda) \quad (2)$$

Where, L and F_o, respectively, are the upwelling radiance and extraterrestrial solar irradiance at the top of the atmosphere, and μ_o is the cosine of the solar zenith angle, θ_o

To simulate the TOA reflectances, we used a modified version of Ahmad-Fraser's code (1982). The code properly accounts for the Fresnel reflection from the rough ocean surface as well as all order of scattering and polarization of the diffuse radiation in the atmosphere. It can simulate reflectance for any wavelength in the UV, visible, or near-IR part of the spectrum. For this study, we selected the visible bands of SeaWiFS and MODIS sensors. Table 1 shows band-average values of Rayleigh scattering optical thickness, $\tau(\lambda)$, and NO_2 cross-section, σ, for the visible and near IR bands of the two instruments.

Table 1. The Rayleigh scattering optical thickness (τ) and NO_2 (σ) absorption cross-section (10^{-19}) per molecule for the SeaWiFS and the MODIS-aqua visible and near IR bands.

SeaWiFS											
Band(*nm*)	412	443	490	510	555	670	765	865	-	-	-
τ(Rayl.)	0.3136	0.2346	0.1546	0.1330	0.0947	0.04450	0.0256	0.0169	-	-	-
$\sigma(NO_2)$	5.915	4.913	2.667	1.995	0.874	0.085	0.080	0.000	-	-	-
MODIS											
Band(*nm*)	412	443	469	488	531	551	555	645	667	670	748
τ(Rayl.)	0.3092	0.2363	0.1911	0.1590	0.1126	0.0990	0.0943	0.0508	0.0444	0.0415	0.0285
$\sigma(NO_2)$	7.724	4.916	3.897	2.802	1.437	1.124	0.877	0.070	0.080	0.090	0.10

In our RT simulations, the aerosols size distribution is characterized by a bi-modal lognormal distribution (C80) and these aerosols are distributed vertically according to Elterman's (1964) distribution. C80 is similar to coastal aerosol distributions that are used operationally for the atmospheric correction of the SeaWiFS and MODIS data. It is constructed from Shettle and Fenn's (1979) tropospheric and Oceanic models for a relative humidity value of 80 percent.

We use five NO_2 profiles in the RT simulations. Three of these profiles are constructed by combining the mean stratospheric NO_2 profile obtained from Goddard Chemical Transport Model (CTM) with three tropospheric NO_2 profiles obtained from Global Earth Observing System CHEMistry (GEOS-CHEM) 3-D model representing low, moderate and high amounts of NO_2 pollution. Two additional tropospheric NO_2 profiles are created by averaging the low and moderate, and the moderate and high tropospheric NO_2 profiles. The amounts of NO_2 in the five profiles are, respectively, 2.847×10^{15}, 3.069×10^{15}, 3.291×10^{15}, 7.301×10^{15} and 1.132×10^{16} molecules/cm^2. Three of these profiles are shown in Figure 1.

The lower boundary of our model atmosphere is a rough ocean surface where it is assumed that the slope probability distribution of the capillary-waves follow Cox and Munk (1954) wind-direction independent distribution. This distribution is characterized by wind speed alone. A wind speed of 4m/sec is used in the simulations.

Finally, we carry out the simulations for a molecular atmosphere, and molecular plus aerosol atmosphere in the absence of NO_2 gas, and then repeated the simulations with all the NO_2 profiles described above. In these simulations, the contributions from water-leaving radiances and white caps are not considered.

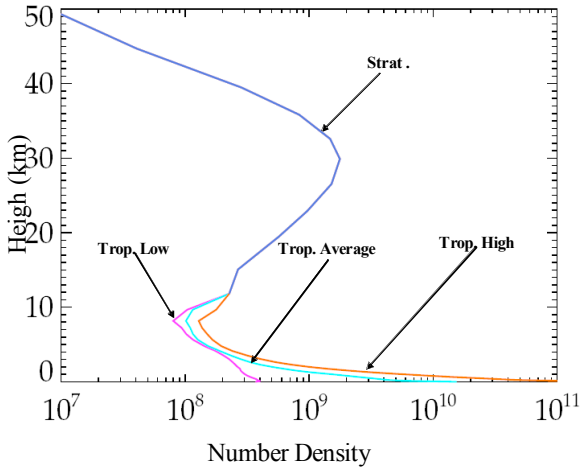

Figure 1. NO_2 profiles used in the RT simulations.

RESULTS

Although, RT simulations are performed for all bands of SeaWiFS and MODIS listed in Table 1, we report here the results for the 412-nm band only. This band has the largest value of NO_2 absorption cross-section and largest value of the Rayleigh optical thickness, and, therefore, shows the largest change in the TOA reflectance. Other bands, to a lesser degree, show similar results. Figure 2a shows the TOA reflectance for a molecular and molecular plus aerosol models of atmosphere. For both models of the atmosphere, the reflectance increases with an increase in the view and the solar zenith angles. In addition, the TOA reflectance increases with aerosols in the atmosphere, however, only by ~10 percent. Also, the increase is very weakly dependent on the view angle. The increase in the reflectance with view and solar zenith angles can be understood by realizing that the increase in the values of these two angles increases the slant path and, hence the 'scattering centers', in the atmosphere. Similarly, addition of aerosols further increases the scattering centers but aerosols, because of their smaller values of the phase function in the backward directions, are not as efficient scatters as the air molecules. Figure 2b shows the effect of NO_2 absorption on the TOA reflectance, where the ordinate is the ratio of reflectance with and without NO_2 in the model atmosphere. As

expected, the TOA reflectance decreases with an increase in NO_2 amount and the rate of decrease is larger for $\theta_o=60^o$ than for $\theta_o=30^o$. This is because of larger slant path for $\theta_o=60^o$, which results in more scattering and, hence, more absorption. We also note that the relative decrease in the TOA reflectance is practically independent of the aerosol amount in the atmosphere. This suggests that we can develop an atmospheric correction algorithm that does not require a priori knowledge of aerosols properties in the atmosphere.

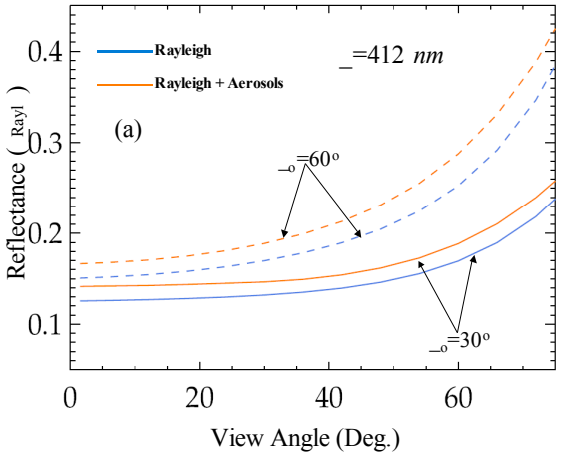

Figures 2a. Top-of-Atmosphere (TOA) reflectances for a molecular, and molecular plus aerosol models of atmosphere with a rough ocean surface at the lower boundary. An aerosol optical thickness of 0.2 is used in the simulations. Simulations for $\theta_o=30^o$ are represented by solid lines and for $\theta_o=60^o$ by dashed lines.

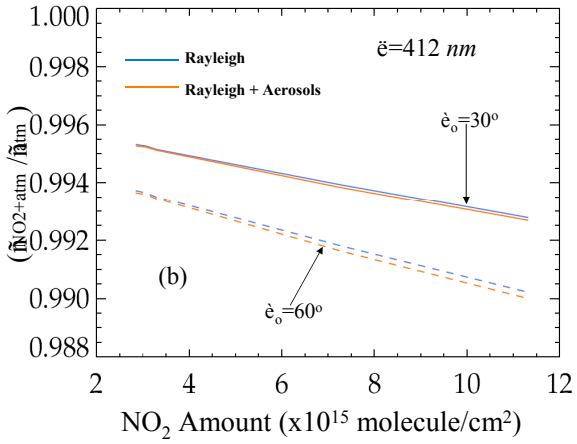

Figure 2b. Ratio of TOA reflectances with and without NO_2 in the models of atmosphere as a function of NO_2 amount. Other details are same as in Figure 2a.

The azimuth dependence of the relative change in the TOA reflectance with and without NO_2 in the atmosphere is shown in Figures 3a and 3b. These results are for a highly NO_2 polluted ($1.13x10^{16}$ molecules/cm^2) molecular atmosphere. We find that the relative change in the TOA reflectance is almost independent of the azimuth angle. We also find similar results when aerosols are added to the atmosphere. We will use these results later in developing the atmospheric correction algorithm, which is described below.

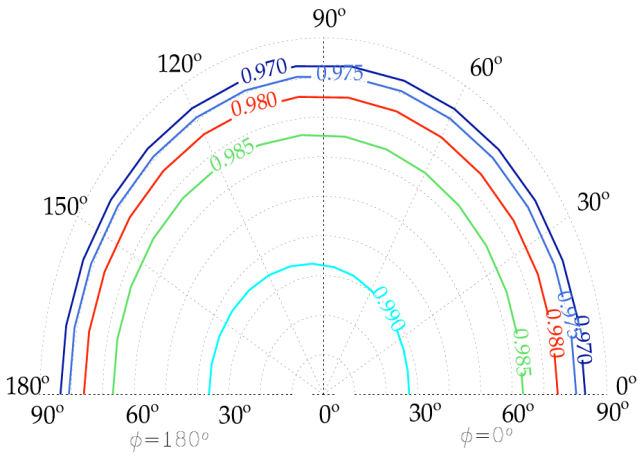

Figure 3a. Ratio of TOA reflectances with and without NO_2 for a molecular atmosphere for θ_o=30°

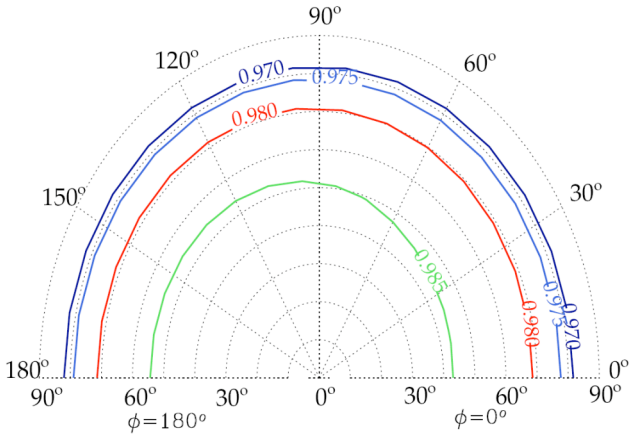

Figure 3b. Same as in Figure 3a but for θ_o=60°

NO_2 CORRECTION ALGORITHM

For most absorbing gases that reside in the stratosphere or upper troposphere, a simple Beer's law correction is sufficient to remove the effect of absorption from the reflectance measured at TOA. The Beer's law correction can be written as:

$$\rho_{corr} = \rho_{obs}\exp[\alpha N(\sec\theta_o+\sec\theta)] \qquad (3)$$

Where α and N are, respectively, the absorption cross-section and column amount of the absorbing gas; ρ_{obs} and ρ_{corr} are, respectively, TOA reflectance with and without the absorbing gas, and ($\sec\theta_o$+ $\sec\theta$) is the geometric air mass factor (AMF). For an absorbing gas that resides in the lower troposphere, an atmospheric correction algorithm solely based on geometric AMF is not sufficient. This is because the absorption increases with multiple scattering by air molecules and aerosols in the atmosphere. For stratospheric absorbing gases, the use of the geometric AMF is valid because the effect of additional absorption due to scattering by air molecules is very small and in most cases can be ignored.

In the presence of tropospheric absorbing gases, it is important that we determine the AMF through the radiative transfer simulation. For this purpose, we re-write Equation 3 as:

$$\text{AMF} = ln(\rho_{corr}/\rho_{obs})/\alpha N \qquad (4)$$

To compute the AMF for the NO_2 gas, we used the RT simulations for molecular atmosphere with the five NO_2 profiles described earlier in this paper. Based on the results presented in the preceding section, the AMF determined for molecular atmosphere is equally applicable for molecular atmosphere with aerosols. It should be noted that radiative transfer derived AMF depends on the Sun-view-angle geometry and the vertical profile of the NO_2 in the atmosphere. Also, based on the results presented in

Figures 3a and 3b, we can ignore the azimuth dependence of AMF. In other words, the AMF determined for molecular atmosphere for one value of azimuth angle (for example, $\varphi=96^o$) should be equally applicable for azimuth angles of SeaWiFS and MODIS observation, which are generally larger than 90^o. Of course, the RT-derived AMF will continue to be dependent on view and solar zenith angles and NO_2 vertical profile in the atmosphere. For operational processing of the data, it is more desirable (faster) to use an equation to compute a quantity than use look up tables to determine the value of the quantity. With this in mind, we parameterized the RT-derived AMF for $\varphi=96^o$ using polynomials in $\sec\theta$ and $\sec\theta_o$. We expressed the view angle dependence by a 3^{rd} order polynomial in $\sec\theta$, and then each coefficient by a 5^{th} order polynomial in $\sec\theta_o$.

To test the RT derived AMF correction algorithm, we used the polynomial coefficients derived for the 'average' tropospheric NO_2 and $\varphi=96^o$ and computed the ratio of reflectances with and without NO_2 in the atmosphere. The results for low, average and high tropospheric NO_2 are shown in Figures 4. These results suggest that AMF derived from average tropospheric NO_2 profile will properly correct the TOA reflectances when the NO_2 amount in the troposphere is less than that in the average tropospheric NO_2 profile, but it will overestimate the atmospheric correction when the NO_2 amount in the troposphere is higher than in the average NO_2 tropospheric profile. One reason for this overestimation is the fact that most of the NO_2 in the high tropospheric NO_2 atmosphere are very close to the bottom surface, which has a reflectivity of only a few percent. From the RT point of view, there are only a small number of photons that reach the lower boundary, get reflected and reach the top of the atmosphere. This can be seen from the graph in Figure 5 where the sensitivity, $\Delta\rho_{top}/\Delta NO_2$, of a layer is plotted against height. The sensitivity is often called the weighting function and shows change in the TOA reflectance when NO_2 amount in a layer is perturbed by a small amount. The graph is normalized to unity at its maximum value. This graph clearly shows that TOA reflectance is less sensitive to increases in NO_2 near the bottom boundary of the atmosphere.

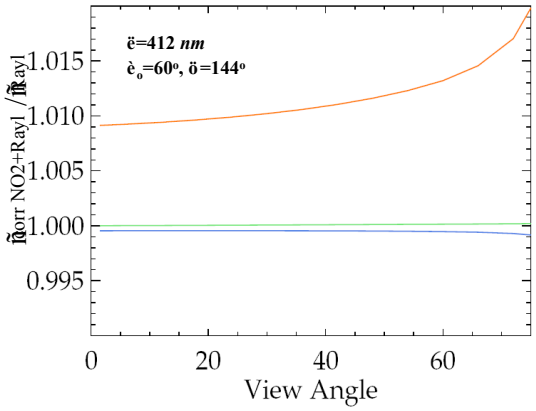

Figure 4. Results of atmospheric correction using RT based AMF computed for a molecular atmosphere with low (blue line, $2.847\text{x}10^{15}$ molecules/cm^2), average (green line, $3.291\text{x}10^{15}$ molecules/cm^2), and high (brown line, $1.132\text{x}10^{16}$ molecules/cm^2) amount of NO_2. The AMF was computed for $\varphi=96^o$.

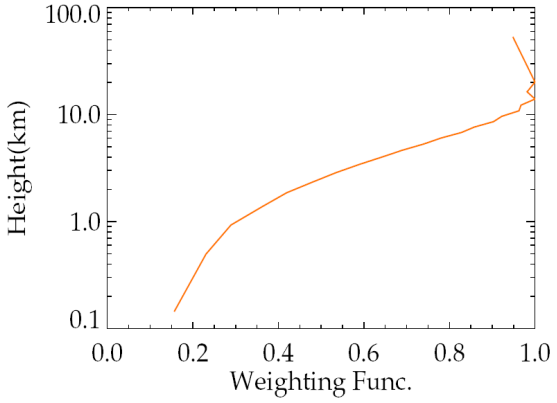

Figure 5. The NO_2 weighting function, $(\Delta\rho_{top}/\Delta NO_2)$, for high amount of NO_2 ($1.132\text{x}10^{16}$ molecules/cm^2) in the atmosphere. The results are for $\theta_o=30^o$

The weighting function results suggest that, to compute the ρ_{corr} from Equation 3, we should not consider the NO_2 amount near surface because the backscattered reflectance, ρ_{obs}, is not sensitive to NO_2 amount near surface. In order to use the Beer's law as described earlier, we decided not to include the amount of NO_2 from 200 meters to the surface in the calculation of ρ_{corr} from Equation 3. The value of 200 meter was selected because it was closer to the value of the top level of the bottom-most-layer in the RT calculations.

For the five NO_2 profiles considered in this paper, we determined the amount of NO_2 from 200 meters to the surface, and examined them as a fraction of the tropospheric NO_2 amount. For this paper, the tropospheric NO_2 amount is the amount of NO_2 from 200 mbar to the surface. This fraction is shown in Figure 6. We find that, for the five tropospheric NO_2 profiles considered here, the $ln[NO_2(200m)]$ is linearly related to $ln[NO_2$ (trop total)].

We applied this new algorithm to the three (low, average and high) tropospheric NO_2 profiles and found that the algorithm works extremely well (*see* Figure 7). The maximum error in all cases was on the order of 0.15 percent. This shows that the correction is practically independent of the view-angle. We find similar results for all solar zenith angles, θ_o, less than 72°.

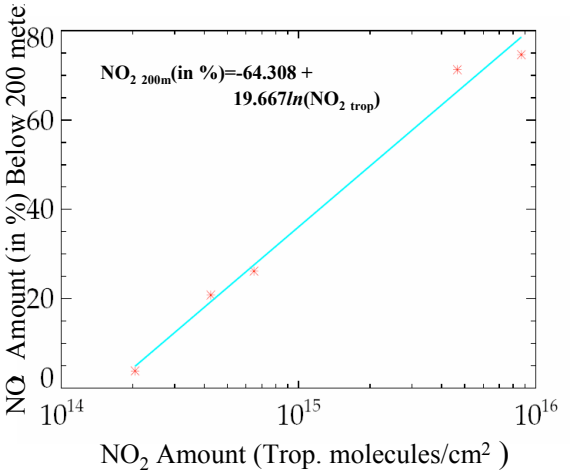

Figure 6. The fraction of NO_2 amount (in percent) from 200 meters to the surface. The abscissa represents the tropospheric amount (from 200 mbar to the surface) of NO_2 in the atmosphere.

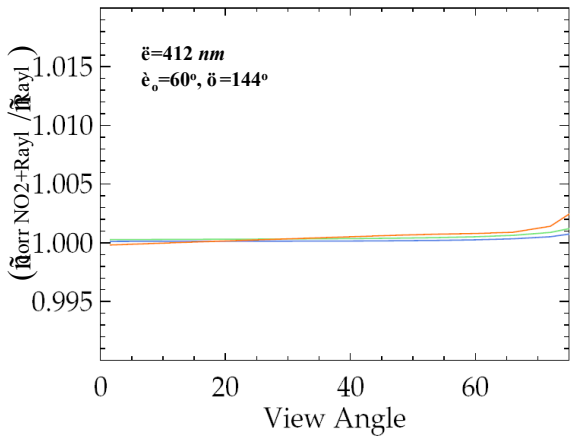

Figure 7. The atmospheric correction with the RT based AMF after correcting for NO_2 amount from 200 meters to the surface. Other details are the same as in Figure 4.

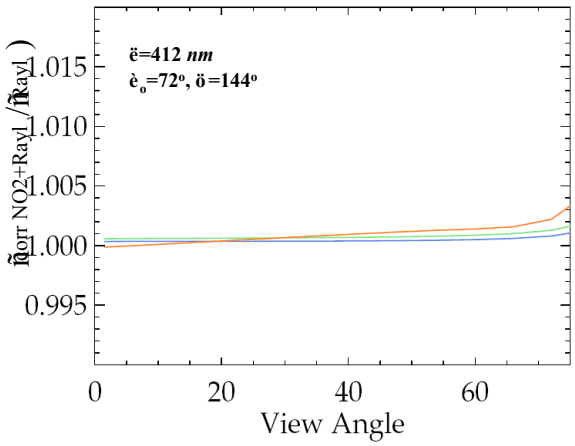

Figure 8 The atmospheric correction with

The idea that we can ignore the NO_2 amount from 200 meters to the surface prompted us to ask whether we can use the corrected NO_2 amount with geometric AMF to accurately determine the TOA reflectance in the presence of high NO_2 amount in the atmosphere. We tested this hypothesis on model atmospheres with the three, low, average and high tropospheric NO_2 amounts and found that this method also produced results that are almost as good as with AMF derived with the help of radiative transfer calculations. The results for $\theta_o=60^o$ is shown in Figure 8. At larger solar zenith angle (for example, $\theta_o=72^o$) we do find a weak view-angle-dependence in the atmospheric correction.

CASE STUDY

We have tested our new NO_2 atmospheric correction algorithm on number MODIS scenes off the Eastern Coast of the USA and found that the correction significantly increases the estimated water-leaving radiance in the 412-nm band of the instrument. We processed the data using both the RT derived AMF and the geometric AMF and found very similar results. The results from one case study using geometric AMF are described below.

We selected MODIS-Aqua data from April 11, 2005 over the Northern Eastern Coast of the USA. Figure 9a shows the RGB image, which was produced by combining the radiances from 469, 555 and 645-nm bands of the MODIS instrument. The scene is generally clear, except that there is a dust plume over the ocean that appears to be coming from the New Jersey area. Figure 9b shows the retrieved aerosol optical thickness (AOT) over the same scene in the 869-nm band. We find that the AOT is ~0.2 in the plume, but it is generally less than 0.1 over most of the scene and over some part of the ocean, AOT is ~0.04.

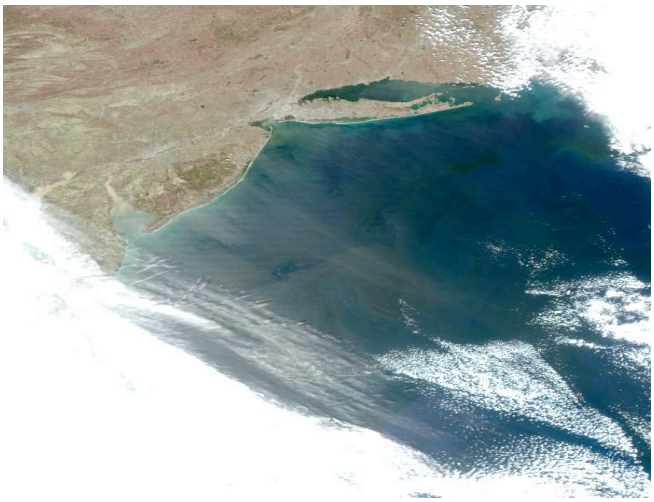

Figure 9a. The RGB image of a MODIS-Aqua scene from April 11, 2005 over the Northern Eastern Coast of the US.

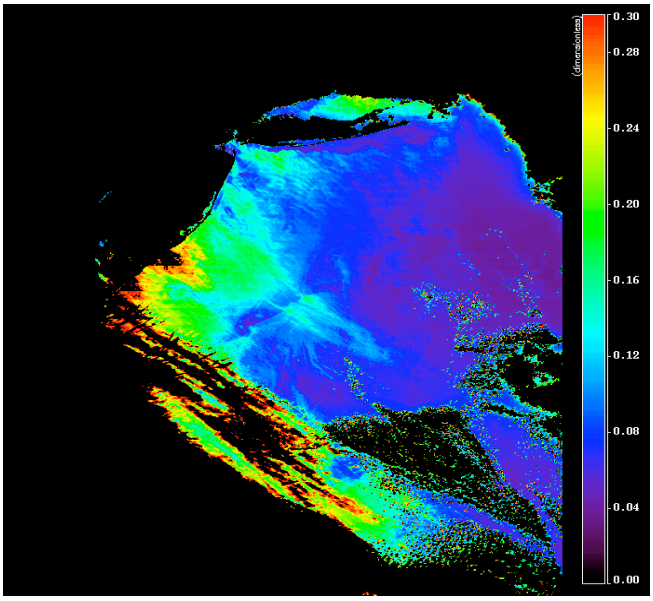

Figure 9b. The 869-nm aerosol optical thickness over Northern Eastern Coast of the USA on April 11, 2005.

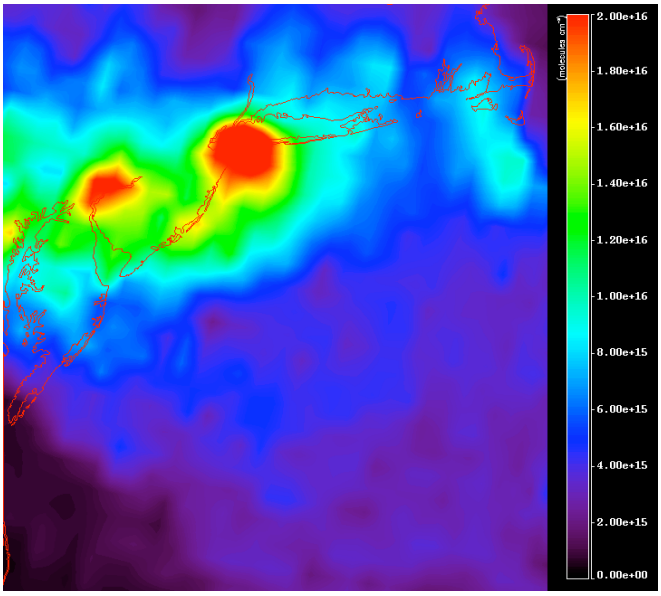

Figure 9c. The tropospheric NO2 amount over Northern Eastern Coast of the USA on April 11, 2005.

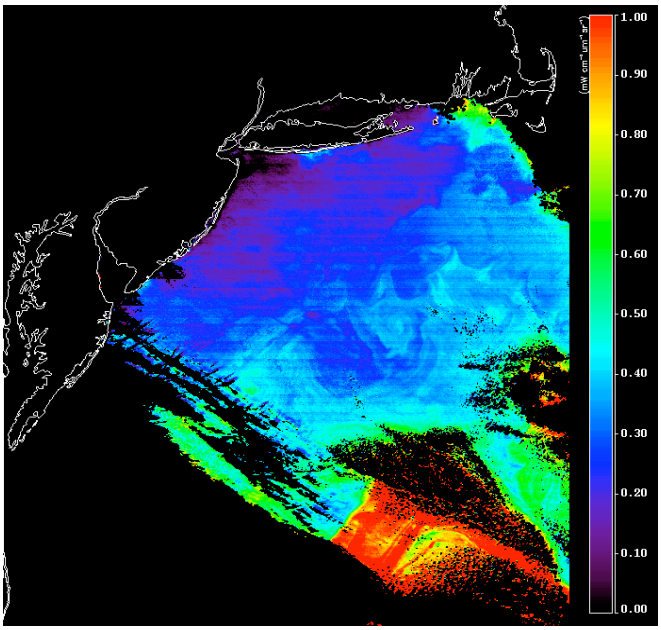

Figure 9d. The 412-nm band normalized water-leaving radiance, nLw, from the current operational algorithm for the MODIS scene shown in Figure 9a.

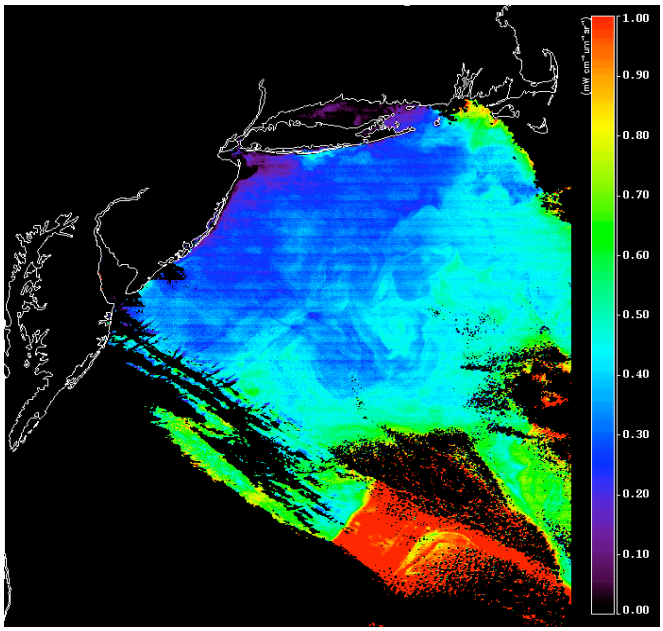

Figure 9e. The 412-nm band normalized water-leaving radiance, nLw, using the NO_2 correction algorithm for the MODIS scene shown in Figure 9a.

The tropospheric NO_2 amounts, shown in Figure 9c, were obtained from the Ozone Measuring Instrument (OMI) onboard MODIS-Aura, which was launched on July 15, 2004 and flies in formation with MODIS-Aqua. The OMI NO_2 data was processed at the Goddard Space Flight Center (GSFC)

and provided by the NO_2 Processing Team. The NO_2 data used in our atmospheric correction algorithm consisted of daily total NO_2 and tropospheric NO_2 amount given at every 0.25x0.25 degree grid. Presently, data from September 29, 2004 to May 14, 2006 are available; however, the current products are provisional in nature.

In the NO_2 image we find NO_2 amounts greater than $2x10^{16}$ molecules/cm^2 over New York City and the surrounding oceanic area. We also find very significant concentrations (~$1x10^{16}$ moelcules/cm^2) over a much larger area of the ocean that extends from Delaware-New Jersey in the south to New York Long-Island in the north. In addition, over most of the cloud free ocean area, the NO_2 amounts are ~$5x10^{15}$ molecules/cm^2.

Figure 9d shows the normalized water-leaving radiance (nLw) in the 412-nm band from the current operational processing of MODIS. Comparing Figure 9c with 9d, we find that in the region where tropospheric NO_2 is very high (>$1.6x10^{16}$ molecules/cm^2), the nLw is very low (< 0.1mW/cm2/μm/sr). Figure 9e shows the same scene with NO_2 atmospheric correction. We find that, nLw values over high NO_2 concentration areas (Figure 9c), are now elevated. Also, the region with very small value of nLw (<0.1mW/cm2/μm/sr) in Figure 9d has practically disappeared.

To get a general sense of the shift in nLw for the 412-nm band radiance, we show, in Figure 10, a histogram of nLw radiances with and without NO_2 correction. For this scene, the peak of the distribution in the operational version is around 0.35 mW/cm^2/μm/sr and with the NO_2 correction, the peak shifts to 0.45 mW/cm^2/μm/sr. This suggests that, in the coastal areas under high NO_2 amount, the current operational processing underestimates the nLw for the 412-nm band by 22 percent.

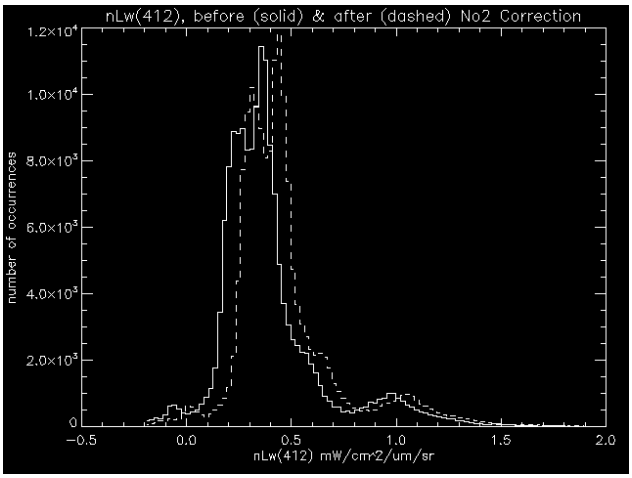

Figure 10. Histogram of 412-nm band water-leaving radiance with (dashed line) and without NO_2 (solid line) correction for the MODIS scene shown in Figure 9a.

CONCLUSIONS

We have presented the details of an atmospheric-correction algorithm that allows accurate retrieval of water-leaving radiances in the presence of varying amount of NO_2 in the atmosphere over ocean. The correction algorithm is based on Beer's law and utilizes the OMI-derived NO_2 values, which are corrected for the boundary layer NO_2 (200 meters to the ground). The boundary layer correction is obtained from a simple empirical relation that is derived from the tropospheric NO_2 profiles obtained from GEOS-CHEM 3-D model. Our analyses show that, with the boundary layer correction, the Beer's law with geometric AMF gives results as good as obtained from the RT based AMF. Finally, in the Chesapeake Bay area, our NO_2 correction algorithm reduces the number of negative water-leaving

(nLw) estimates in the 412-nm band of MODIS data, and increases the nLw in the same band by almost 22 percent.

Acknowledgements

We thank the NO_2 processing team, in particular, Drs. J. F. Gleason, M. O. Wenig and E. A. Celarier for providing the NO_2 data.

References

Ahmad, Z., and R. S. Fraser, An iterative radiative transfer code for ocean-atmosphere systems, *J. Atmos. Sci*., 39, 656-665, 1982.

Bucsela, E. J., E. A. Celarier, M. O. Wenig, J. F. Gleason, J. P. Veefkind, K. F. Boersma, and E. J. Brinksma, *IEEE Trans. Geosci. Remote Sensing*, 44(5), 1245-1258, 2006.

Elterman, J., Parameters for attenuation in the atmospheric windows for fifteen wavelengths. *Appl. Opt*., 3, 745-749, 1964.

Gordon, H. R., Atmospheric correction of ocean color imagery in the Earth Observing System era, *J. Geophys. Res*., **102**, 17081-17106, 1997.

Shettle, E. P., and R. W. Fenn, Models for the Aerosols of the Lower Atmosphere and the Effect of the Humidity Variation on Their Optical Properties, Rep. AFGL-TR-79-0214, U. S. Air Force Geophysical Laboratory, Hancom Air force Base, Mass., 1997.

Solomon, S., R. W. Portmann, R. W. Saders, J. S. Daniel, D. W. Madsen, B. Bartram, and E. G. Dutton, On the role of nitrogen dioxide in the absorption of the solar radiation, *J. Geophys. Res*., 99(D10), 12047-12058, 1999.

Thuillier, G., M. Herse, P. C. Simon, D. Labs, H. Mandel, D. Gillotay, and T. Foujols, The solar spectral irradiance from 200 to 2400 nm as measured by the SOLSPEC spectrometer from the ATLAS 1-2-3 and EURECA missions, *Solar Physics*, 214(1), 1-22, 2003.

Vandaele, A. C., C. Hermans, P. C. Simon, M. Carleer, R. Colin, S. Folly, M. F. Merienne, A. Jenouvrier, and B.Coquart, Measurements of the NO2 absorption cross-section from 42000 cm-1 to 10000 cm-1 (238-1000 nm) at 220 K and 294 K, *J. Quant. Spectrosc. Radiat. Transf*., 59, 171-184, 1998.